Iterative Reconstruction of SPECT data with Adaptive Regularization

Cyril Riddell, Irene Buvat, Annarita Savi, Maria-Carla Gilardi and Ferrucio Fazio

***Abstract*-- A least-square reconstruction criterion is proposed for simultaneously estimating a SPECT (Single Photon Emission Computed Tomography) emission distribution corrected for attenuation together with its degree of regularization. Only a regularization trend has to be defined and tuned once for all on a reference study. Given this regularization trend, the precise regularization weight, which is usually fixed *a priori*, is automatically computed for each data set to adapt to the noise content of the data. We demonstrate that this adaptive process yields better results when the noise conditions change than when the regularization weight is kept constant. This adaptation is illustrated on simulated cardiac data for noise variations due to changes in the acquisition duration, in the background intensity and in the attenuation map.**

I. Introduction

Today's SPECT tomographs are multi-headed devices equipped with a transmission source that allow for the measurement of the emission distribution of a patient together with its attenuation characteristics [1-3]. Attenuation correction can thus be performed, which is essential to the quantification of SPECT studies [4-6]. Iterative algorithms are compulsory for reconstructing images from SPECT data with the aim of quantification using attenuation correction [7]. Iterative methods present some drawbacks such as the noise amplification as the number of iterations increases. To prevent from large noise amplification, regularization is often used, and the resulting solution is then a trade-off between fidelity to the measured data and bias due to the regularity of the solution constrained through the regularization term [8]. This implies that a regularization parameter is set a priori, in a way that optimizes this trade-off for a given situation. This regularization parameter may then be kept unchanged for all the patients enrolled in a given protocol, considering that conditions do not differ much from one study to another. This is only partially true, since activity distribution and noise characteristics do vary amongst patients. According to the size and physiology of the patient, more or less photons are detected for constant acquisition conditions. The total duration of a scan can be adjusted to compensate for this diversity, but this results in the variation of the acquisition conditions themselves.

In the following study, we describe a technique for simultaneously estimating the regularized least-square solution of a SPECT reconstruction problem with its degree of regularization to automatically find an appropriate trade-off between noise and bias as the noise in the data changes.

II. Theory

An image is estimated from a finite set of SPECT attenuated measurements by solving a linear system such as:

$$R_a f = s \qquad (1)$$

where f is the unknown image vector, s is the attenuated SPECT sinogram and R_a is a matrix that models a SPECT tomographic acquisition with non-uniform attenuation. We propose a least-square approach based on the following normal equations:

$$T^t DTx = T^t Ds \qquad (2)$$

where $T = R_a \Gamma$ is the attenuated Radon transform R_a normalized by the Chang correction Γ [9] and D stands for the ramp filtering operation. The symbol T^t denotes the transpose matrix of T. The vector x is the new unknown and is defined such that $f = \Gamma x$, to preserve the system symmetry. The ramp filter and the Chang correction are used as a preliminary approximate inversion making the matrix $T^t DT$ close to the identity matrix, in order to speed convergence up and work with normalized operators [10].

Eq. (2) leads to the following least-square minimization problem [11]:

$$\min_x \left\{ \varphi(x) = \left\| D^{1/2} (Tx - s) \right\|^2 \right\}. \qquad (3)$$

A regularization term $\rho(x)$ is added to avoid noise amplification by constraining the norm of the image gradient ∇x:

$$\rho(x) = \left\| \nabla x \right\|^2 = \left\langle \Delta x, x \right\rangle \qquad (4)$$

where Δ stands for the normalized Laplacian operator and $\langle , \rangle$ stands for the dot product. The following regularizing least-square functional is obtained:

$$M(x) = \varphi(x) + \alpha\rho(x). \qquad (5)$$

For a given strictly positive α, this functional has a unique minimum that is a compromise between fidelity to

C. Riddell is with GE Medical System, Buc, France (e-mail: Cyril.Riddell@med.ge.com).

I. Buvat is with the U494 INSERM, CHU Pitie-Salpetriere, Paris, France (telephone: 33-1-53 82 84 15, e-mail: buvat@imed.jussieu.fr).

Annarita Savi, Maria-Carla Gilardi and Ferrucio Fazio are with the INB-CNR, Ospedale H San Raffaele, Milan, Italy.

0-7803-7324-3/02/$17.00 © 2002 IEEE

the data (measured by the term $\varphi(x)$) and regularity of the solution (measured by the term $\rho(x)$). It is possible to simultaneously estimate an image and its degree of regularization, by making an explicit dependence between them [12]. The simultaneous estimation is obtained by finding the minimum of:

$$M(x,\alpha(x)) = \varphi(x) + \alpha(x)\rho(x) \qquad (6)$$

under the constraint of a *linear* relationship between the regularization parameter and the regularizing functional:

$$\alpha(x) = \gamma M(x,\alpha(x)) . \qquad (7)$$

This relationship makes $\alpha(x)$ proportional to $\varphi(x)$ and $\rho(x)$ which both increase when the noise in the data increases. The value of γ can be set such that the function $\alpha(x)$ is monotonically increasing, mapping R^n into $[0,+\infty[$ and such that the functional M is convex with a unique minimum.

The minimum of M with respect to α coincides with the minimum of M with respect to x and is found by solving:

$$\begin{cases} T^t DTx + \alpha(x)\Delta x = T^t Ds \\ \alpha(x) = \varphi(x) \Big/ \left(1/\gamma - \rho(x)\right) \end{cases} . \qquad (8)$$

This system can be solved with a successive approximation scheme [12]. However, much faster convergence is obtained when using the conjugate gradient algorithm. To apply the conjugate gradient to this non-linear problem, $\alpha(x)$ is estimated at each iteration but changed only if the new estimate of α is different enough from its current value. When $\alpha(x)$ is updated, the conjugate gradient is restarted from the current estimate of the distribution to solve the system defined by the new value of α. A similar trick was used by Kaufman for applying a positivity constraint with the conjugate gradient [13].

In this approach, the regularization strength α is modulated by the value of γ that we call the regularization "trend" in the following. Our strategy involves setting this regularization trend γ so that the algorithm produces a given regularization strength α for a reference study, for which this regularization strength is optimized. Then, solving system (8) must produce a decreased (resp. increased) regularization strength when the acquisition conditions are improved (resp. degraded) while γ is left unchanged. In order to keep γ constant whatever the true distribution x^*, γ must be normalized by $\|x^*\|^2$. Since x^* is unknown, its norm is estimated by:

$$\langle x^*, x^* \rangle = \langle T^t DTx^*, x^* \rangle = \langle Ds, s \rangle . \qquad (9)$$

III. Experiments

A segmented CT slice from the Zubal phantom at the heart level was considered [14]. The simulated activity distribution was obtained by setting the heart muscle to 10 counts/sec., the blood pool to 3, the lungs to 2 while all other tissues were merged into a uniform background set to 1 (Fig. 1, image A). The image was projected in parallel geometry over 360° with 120 steps (bin size 4 mm), by taking attenuation into account. The attenuation map was taken as the non-segmented CT slice (Fig 1, image B) scaled to mimic attenuation undergone by Tc^{99m} photons (attenuation of 0.15 cm^{-1} in water) and by Tl^{201} photons (attenuation of 0.17 cm^{-1} in water). With Tc^{99m}, the total activity in the sinogram was equal to 2675 counts/sec. Four levels of noise were considered, corresponding to acquisition times of 50, 100, 200, and 500 seconds. Two additional variations were introduced: a) background and lungs values were zeroed and b) background and lung values of the original distribution were doubled. In total, 24 configurations were thus considered (3 activity distributions x 4 acquisition durations x 2 attenuation maps).

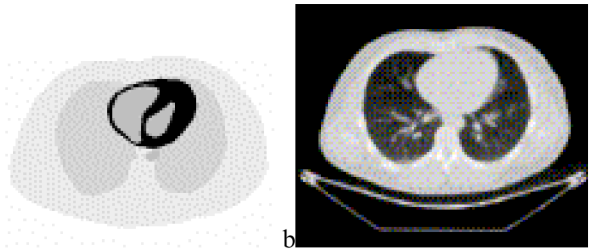

a b

Fig. 1. Emission (a) and transmission (b) images used for the simulation of noise-free SPECT data.

Two regularization approaches were compared: fixed regularization (FR), i.e. the conjugate gradient applied to eq. (5), and adaptive regularization (AR), i.e. the conjugate gradient applied to eq. (8). For a given data set, $\varepsilon(\alpha)$ could be calculated using the conjugate gradient with FR, by varying α step by step. On the other hand, AR automatically determined $\varepsilon(\alpha)$ for any data set, once γ was fixed. To set the regularization trend, a particular configuration was considered, corresponding to a 100 sec. acquisition time with the Tc^{99m} attenuation map and the non-specific activity consisting of 2 in the lungs and 1 in the background. For this study, the α value minimizing the normalized mean square error (NMSE) between the estimated activity distribution and the true activity distribution was found equal to 0.99. The corresponding γ was deduced and was equal to 3.0. This fixed γ was then considered to process all other 23 configurations, leading to a different α value for each configuration.

Given the known emission distribution x^*, noise and bias in a reconstructed image x' were characterized by calculating the normalized mean square error (NMSE) between the estimated activity distribution and the true activity distribution:

$$\varepsilon = 10000. \|x' - x^*\|^2 \Big/ \|x^*\|^2 . \qquad (10)$$

For all 24 data sets, we computed the NMSE error of the solution generated by AR, and compared this error to the lowest NMSE as obtained using the conjugate gradient with FR with α varying by steps of 0.1.

IV. RESULTS

Tables I to IV show the performances of adaptive regularization for $\gamma = 3.0$: for all acquisition times (1st column), the regularization values α_{AR} obtained by solving system (8) with the conjugate gradient are given in the 2nd column together with the corresponding NMSE, denoted ε_{AR} in the 3rd column. FR was used to find the lowest NMSE, denoted ε^*, that is given in the 4th column. The NMSE that would be obtained if α were kept fixed to 0.99 whatever the data set is denoted ε_{FR}. The last two columns indicate the respective performances of AR and FR by giving the percentage difference between the automatically found ε_{AR} value and the optimal ε^* and between the NMSE ε_{FR} corresponding to the fixed regularization parameter and the optimal ε^*.

Table I shows the results obtained with the Tc^{99m} attenuated data with a background of 1 and lung values of 2. As expected, AR increased the regularization parameter for the acquisition duration of 50 sec. that was shorter than that used for optimizing γ (the data set used for the optimization was 100 sec. in duration). On the other hand, the regularization parameter decreased when considering acquisition durations greater than 100 sec. as the data got less noisy. For all acquisition times, the NMSE corresponding to the regularization parameter automatically found using AR was very close to the smallest NMSE that could be found by manually optimizing α. AR yielded regularization values more than 4 times higher for the shortest acquisition duration compared to the longest acquisition duration. When keeping the regularization value of 0.99 constant for all data sets, the resulting NMSE was higher than the optimal NMSE by as much as 27%.

TABLE I
ADAPTIVE REGULARIZATION FOR TC99M ATTENUATED DATA, WITH A BACKGROUND VALUE OF 1 AND LUNG VALUES OF 2

Acq. duration	α_{AR}	ε_{AR}	ε^*	$\frac{(\varepsilon_{AR}-\varepsilon^*)}{\varepsilon^*}$	$\frac{(\varepsilon_{FR}-\varepsilon^*)}{\varepsilon^*}$
50	1.42	867	861	1%	8%
100	0.99	652	652	0%	0%
200	0.63	532	532	0%	3%
500	0.36	365	365	0%	27%

Table II illustrates the automatic changes in α for changes in the processed data sets induced by considering the attenuation map corresponding to Tl^{201} instead of Tc^{99m}. As photons emitted by Tl^{201} are more attenuated by the human body than photons emitted by Tc^{99m}, the Tl^{201} data were noisier than the Tc^{99m} data for the same acquisition duration. Therefore, an increase of the regularization values was expected compared to those obtained for Tc^{99m} (Table I), for the same acquisition durations. Table II demonstrates this behavior, with regularization values varying from 0.40 to 1.54 for 500 sec. to 50 sec. acquisition durations for Tl^{201} data, to be compared with regularization values varying from 0.36 to 1.42 for Tc^{99m}. NMSE were within 2% of the lowest NMSE in each case, whereas when using fixed regularization, NMSE greater than the lowest NMSE by up to 15% were observed.

TABLE II
ADAPTIVE REGULARIZATION FOR TL201 ATTENUATED DATA, WITH A BACKGROUND VALUE OF 1 AND LUNG VALUES OF 2

Acq. duration	α_{AR}	ε_{AR}	ε^*	$\frac{(\varepsilon_{AR}-\varepsilon^*)}{\varepsilon^*}$	$\frac{(\varepsilon_{FR}-\varepsilon^*)}{\varepsilon^*}$
50	1.54	942	928	2%	9%
100	1.10	717	710	1%	3%
200	0.74	596	593	0%	1%
500	0.40	436	436	0%	15%

Table III shows the performance of AR for Tc^{99m} attenuated data when background and lungs values were set to zero while they were different from zero in the configuration used for optimizing γ. Without background, the data were less noisy as a zero background appears in the data as zeroes with a variance equal to zero. Therefore, for a given attenuation duration, the regularization parameter was expected to be smaller than for the same data including a background (Table I). This is what was actually observed, and the NMSE corresponding to the AR reconstruction were always of the same order (for the 50 sec. acquisition time) or smaller than those obtained using the FR reconstruction. However, the regularization value that yielded the minimum NMSE was never reached.

TABLE III
ADAPTIVE REGULARIZATION FOR TC99M ATTENUATED DATA, WITH BACKGROUND AND LUNG VALUES EQUAL TO ZERO

Acq. duration	α_{AR}	ε_{AR}	ε^*	$\frac{(\varepsilon_{AR}-\varepsilon^*)}{\varepsilon^*}$	$\frac{(\varepsilon_{FR}-\varepsilon^*)}{\varepsilon^*}$
50	1.02	854	834	2%	1%
100	0.66	719	703	2%	10%
200	0.41	564	552	9%	29%
500	0.27	417	381	9%	76%

Table IV shows the AR results when lung and background activities were twice as much as those of the study used to set the calibration trend.

TABLE IV
ADAPTIVE REGULARIZATION FOR TC99M ATTENUATED DATA, WITH BACKGROUND VALUE OF 2 AND LUNG VALUES OF 4

Acq. duration	α_{AR}	ε_{AR}	ε^*	$\frac{(\varepsilon_{AR}-\varepsilon^*)}{\varepsilon^*}$	$\frac{(\varepsilon_{FR}-\varepsilon^*)}{\varepsilon^*}$
50	1.21	626	555	13%	20%
100	0.82	480	450	7%	3%
200	0.51	399	369	8%	0%
500	0.30	297	286	4%	12%

In that instance, AR yielded smaller regularization values than those obtained when the background and lung activities were half (Table I). This is because increasing the background and lung activities changed the structures in the images, and did not simply correspond to a change of the noise in the data. However, the change in regularization value with respect to the acquisition duration was consistent. When comparing

to the NMSE obtained for a fixed regularization value, AR yielded more homogeneous results for the different acquisition durations, with NMSE 4% to 13% higher than the optimal NMSE, while NMSE were 0% to 20% higher than the optimal NMSE with fixed regularization.

Figure 2 displays the images corresponding to the results presented in Table I. The images corresponding to a regularization trend of 3 (second row) led to a more uniform image quality for the different acquisition durations than the fixed regularization (third row). The higher the regularization trend ($\gamma = 5$, first row), the less variations in image quality for different levels of noise in the data.

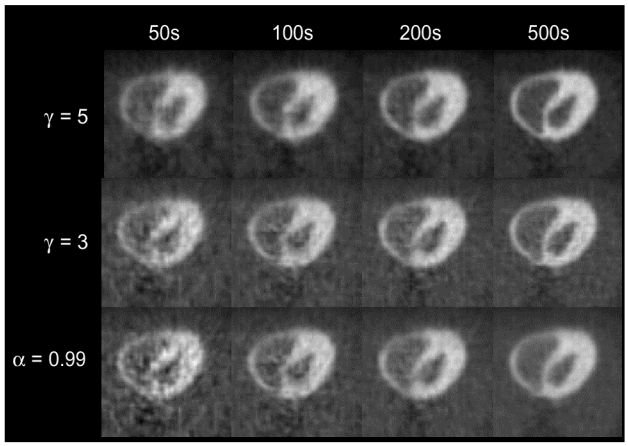

Fig. 2. Tc^{99m} attenuated data and original background and lung values. Heart muscle reconstruction with fixed regularization ($\alpha = 0.99$, bottom row) and adaptive regularization ($\gamma = 3.0$ middle row and $\gamma = 5.0$ top row).

V. Discussion

Adaptive regularization was demonstrated for SPECT reconstruction with attenuation correction with a least- square criterion based on the approximate inversion of the attenuated Radon transform using the Chang correction and the ramp filter. This criterion allowed for the simultaneous estimation of the activity distribution together with its degree of regularization, according to the method proposed by Kang and Katsaggelos [12].

By setting the regularization trend using a reference study, results close to the optimal results, in terms of NMSE, were obtained when varying the acquisition duration and the attenuation map. Even when the background intensity varied, resulting NMSE were within 9% of the minimum NMSE when zeroing the background and within 13% when the background and lungs activities were doubled.

In all cases, adaptive regularization led to more uniformity in the image quality with respect to noise changes due to variations in acquisition duration.

The proposed regularization functional sets a linear relationship between the regularization parameter and the functional itself, to make the minimization problem tractable. This linear dependency might not be strong enough to obtain a regularization parameter yielding an NMSE almost identical to the optimal NMSE, especially when large variations occur between two data sets (as when the background and lung activities were multiplied by two with respect to the background and lung values in the data set used to set the optimization trend). There might be other relationships that adapt more precisely to such variations. Further work is needed to see if this adaptive technique can be implemented for statistical criteria modeling the Poisson noise of the data, such as those in maximum-likelihood expectation-maximization or weighted least-square algorithms, and for alternative regularization constraints that could preserve the edges of the distribution.

To demonstrate that the technique could lead to optimal noise/bias trade-off, we only used simulated data for which the true activity distribution was known. Further evaluation on clinical data is needed to determine whether setting the regularization trend instead of the regularization parameter could reduce the variability of image quality in patients and facilitate the clinical interpretation of attenuation corrected SPECT images.

VI. Conclusion

Adaptive regularization for SPECT non-uniform attenuation correction was tested for four different acquisition durations, three background intensity levels and two attenuation conditions. By setting the regularization trend on a given reference study, the adaptive regularization decreased (resp. increased) the regularization when the acquisition duration increased (resp. decreased) to yield trade-off between noise and bias that were almost independent from the original noise level in the projections. Adaptive regularization was also obtained when changing the attenuation map and the background intensity with respect to the reference study, but strong structural changes in the activity distribution did not lead to optimal trade-off in terms of the NMSE.

Adaptive regularization was demonstrated to be a practical way of modulating the level of filtering according to the noise present in the data in order to generate a more homogeneous image quality from patient to patient.

VII. References

[1] R.J. Jaszczak, D.R. Gilland, M.W. Hanson, S. Jang, K.L. Greer, and R.E. Coleman, "Fast transmission CT for determining attenuation maps using a collimated line source, rotatable air-copper-lead attenuators, and fan-beam collimation," *J. Nucl. Med.*, vol. 34, pp. 1577-1586, 1993.

[2] P. Tan, D.L. Bailey, S.R. Meikle, S. Eberl, R.R. Fulton, and B.F. Hutton, "A scanning line source for simultaneous emission and transmission measurements in SPECT," *J. Nucl. Med.*, vol. 34, pp. 1752-1760, 1993.

[3] G.T. Gullberg, H.T. Morgan, G.S.L. Zeng, P.E. Christian, E.V.R. Di Bella, C.H. Tung, P.J. Maniawski, Y.L. Hsieh, and F.L. Datz, "The design and performance of a simultaneous transmission and emission tomography system," *IEEE Trans. Nucl. Sci.*, vol. 45, pp. 1676- 1698, 1998.

[4] E.P. Ficaro, J.A. Fessler, R.J. Ackerman, W.L. Rogers, J.R. Corbett, and M. Schwaiger, "Simultaneous transmission-emission Thallium-201 cardiac SPECT: Effect of attenuation correction on myocardial tracer distribution," *J. Nucl. Med.*, vol. 36, pp. 921-931, 1995.

[5] E.P. Ficaro, J.A. Fessler, P.D. Shreve, J.N. Kritzman, P.A. Rose, and J.R. Corbett, "Simultaneous transmission/emission myocardial perfusion tomography: Diagnostic accuracy of attenuation-corrected

99mTc-Sestamibi Single Photon Emission Computed Tomography," *Circulation*, vol. 93, pp. 463-473, 1996.

[6] G.N. El Fakhri, I. Buvat, M. Pélégrini, H. Benali, P. Almeida, B. Bendriem, A. Todd-Pokropek, and R. Di Paola, "Respective roles of scatter, attenuation, depth-dependent collimator response and finite spatial resolution in cardiac single-photon emission tomography quantitation: a Monte Carlo study," *Eur. J. Nucl. Med.*, vol. 26, pp. 437-446, 1999.

[7] T.F. Budinger, G.T. Gullberg, and R.H. Huesman, "Emission computed tomography image reconstruction: From implementation to applications," , G.T. Herman, Ed. New-York: Springer, 1979, pp. 147-246.

[8] G. Demoment, "Image reconstruction and restoration: Overview of common estimation structures and problems," *IEEE Trans. Acous., Speech and Signal Processing*, vol. 37, pp. 2024-2036, 1989.

[9] L.T. Chang. "Attenuation correction and incomplete projection in single photon emission computed tomography," *IEEE Trans. Nucl. Sci.*, vol. 26, pp. 2780-2789, 1979.

[10] C. Riddell, B. Bendriem, M.H. Bourguignon, and J.-P. Kernevez, "Approximate inverse and conjugate gradient: non symmetrical algorithms for fast attenuation correction in SPECT," *Phys. Med. Biol.*, vol. 40, pp. 269-281, 1995.

[11] C. Riddell, A. Savi, M.C. Gilardi, and F. Fazio, "Frequency weighted least squares reconstruction of truncated transmission SPECT data," *IEEE Trans. Nucl. Sci.*, vol. 43, pp. 2292-2298, 1996.

[12] M.G. Kang and A.K. Katsaggelos, "General choice of the regularization functional in regularized image-restoration," *IEEE Trans. Image Process*., vol. 4, pp. 594-602, 1995.

[13] L. Kaufman, "Maximum likelihood, least squares, and penalized least squares for PET," *IEEE Trans. Med. Imaging*, vol. 12, pp. 37-51, 1993.

[14] I.G. Zubal, C.R. Harrell, and E. Smith, "Computerized 3D segmented human anatomy," *Med. Phys.*, vol. 21, pp. 299-302, 1994.